J. Nano- Electron. Phys.
3 (2011) No1, P. 1064-1070

PACS numbers: 61.05.cp, 62.23. – c, 78.30.Fs

STRUCTURAL, OPTICAL, AND MAGNETIC PROPERTIES OF $Zn_{1-X}Mn_XS$ (X = 0.00, 0.01, AND 0.03) NANOPARTICLES

S.S. Kanmani, N. Rajkumar, K. Ramachandran

School of Physics, Madurai Kamaraj University,
Madurai-21, India.
E-mail: sskanmani@gmail.com

$Zn_{1-x}Mn_xS$ *(x = 0.00, 0.01, and 0.03) nanoparticles of size ~2 nm were synthesized using a co-precipitation method. Structural characterization by X-Ray diffraction (XRD) measurement revealed that all the synthesized samples were crystallize in the monophasic cubic zinc blende structure and monotonous decrement in the lattice constants with increasing* Mn *content, due to the effective* Mn *doping. The quantum confinement nature of nanoparticles was tested from UV-Vis absorbance measurement and the particle sizes were calculated and compared with XRD. Two emission bands observed in doped nanoparticles were attributed to defect related emission (blue) of* ZnS *and* Mn^{2+} *(orange) respectively, where the intensity of emission peak increases without any significant shift for increase in* Mn^{2+} *concentration. Magnetic measurements showed that all the samples exhibit antiferromagnetic with diamagnetic behavior, at room temperature.*

Keywords: *ZINC BLENDE STRUCTURE, ORANGE AND BLUE EMISSION, LUMINESCENT MATERIAL, MANGANESE DOPING, MAGNETISM.*

(Received 04 February 2011)

1. INTRODUCTION

Due to extensive luminescent properties and higher stability under ambient conditions, ZnS nanomaterials, a II-VI semiconductor with a direct bandgap of 3.6 eV at room temperature and 40 meV as exciton binding energy have a wide range of applications in high-performance displays and devices, phosphors, LEDs, optical sensors, etc., [1, 2]. By doping ZnS with different activating metal ions, one can tune the luminescence properties largely. Among many available wide bandgap compounds, Manganese is well known as an activator for photoluminescence and Bhargava et al. [3] was the first to report the luminescence properties of Mn-doped ZnS nanocrystals prepared by a chemical process at room temperature, which initiated investigation on this topic [4-6]. In particular, ZnS:Mn^{2+} nanomaterials have triggered great interest due to the luminescence enhancement compared to bulk material [3]. These unusual optical properties have contributed to the enhanced interaction between the s-p states of the host (ZnS) and the d states of impurity ions (Mn^{2+}). In addition, the introduction of magnetic Mn^{2+} ions into nonmagnetic ZnS nanoparticles leads to an interesting magnetic and magneto-optical properties in comparison with bulk ZnS:Mn [7]. Wang et al. [8] observed spin-glass behavior at $T_c = 15$ K in $Zn_{1-x}Mn_xS$ at a high concentration $x = 0.32$, but a paramagnetic behavior at a low concentration $x = 0.16$. Heidrich [9] concluded that there is an antiferromagnetic coupling

at the Neel temperature of $T_N = 152$ K, whereas Tsujii et al. [10] found no antiferromagnetic behavior in ZnS:Mn systems. Yuan et al. [11] reported paramagnetic behavior in ZnS:Mn nanosystems prepared by co-precipitation method. As new findings towards spintronic materials, recently in 2008, Lakshmi et al. [12] have reported the existence of room temperature ferromagnetism (RTFM) in nanocrystalline samples of $Zn_{1-x}Mn_xS$ ($x = 0.00$, 0.02, 0.04). Apart from these, there is not much work on ZnS:Mn, particularly, on magnetic properties and most of the papers are focused on the efficient luminescent properties. Here we intend to synthesis $Zn_{1-x}Mn_xS$ ($x = 0.00$, 0.01, and 0.03) nanoparticles for the investigation of its optical as well as magnetic properties.

2. EXPERIMENT

$Zn_{1-x}Mn_xS$ ($x = 0.00$, 0.01, and 0.03) nanoparticles were prepared by co-precipitation method [13]. At first, 0.1 M of zinc acetate dihydrate was dissolved in 100 ml of distilled water and allows it to stir for half an hour. Then, 100 ml aqueous solution of Na_2S (0.1 M) was prepared and added drop wise to the above solution. The obtained precipitate was centrifuged, washed several times with distilled water and ethanol, and dried at 40 °C. Mn doped ZnS nanoparticles were synthesized by using manganese acetate dihydrate as an additional precursor to the above stock solution. The structural analysis of the above synthesized samples were carried out by recording the X-ray diffraction (XRD) spectrum at room temperature using PANalytical X'Pert X-ray diffractometer for 2θ in the range of 10° to 90° with step size of 0.02° using Cu-K_α radiation (wavelength: 1.54056 Å). UV-Vis absorption measurements were carried out at room temperature by using (Shimadzu-2450) UV-Vis absorption spectrometer. The photoluminescence spectra were recorded by using spectroflurophotometer (Shimadzu RF-5000) with an excitation wavelength of 340 nm at room temperature. Infrared spectra of the samples were recorded using a Fourier transmission infrared (FTIR) spectrometer (Shiraz) in the range of 4700 cm^{-1}-340 cm^{-1} with a resolution of 1cm^{-1}, to see whether there is any defect mode appears due to doping. The elemental composition of synthesized materials was carried out by using the energy dispersive X-ray spectrum (EDS) (Nortan System Six, Thermo electron corporation Instrument Super DRY II, USA). The magnetic hysteresis (M-H) loops were measured using vibrating sample magnetometer (Lakeshore-7400) between ± 15 kOe at room temperature.

3. RESULTS AND DISCUSSION

3.1 X- ray diffraction analysis

The XRD patterns of the $Zn_{1-x}Mn_xS$ ($x = 0.00$, 0.01, and 0.03) nanoparticles (Fig. 1) shows three diffraction peak positions correspond to the lattice planes of (1 1 1), (2 2 0), and (3 1 1), matching the cubic zinc blende ZnS structure (JCPDS No. 80-0020). The Mn doping into ZnS has not altered the actual phase and no trace of MnS or secondary phases were observed. Moreover, the diffraction peaks of the formed Mn doped ZnS nanoparticles shifted a little toward the high angle compared with those of undoped ZnS nanoparticles. This suggests that the Mn^{2+} ions substituted into the Zn^{2+}

ions site, resulting in reduced lattice constants. The average particle sizes calculated from the full-width at half-maximum (FWHM) of XRD peaks using Debye–Sherrer formula are ~ 2 nm, which slightly deviates with Mn^{2+} concentration. Lattice parameters were calculated and tabulated in Table 1, which decreases with increase of Mn doping and also from bulk (a = 5.409 Å).

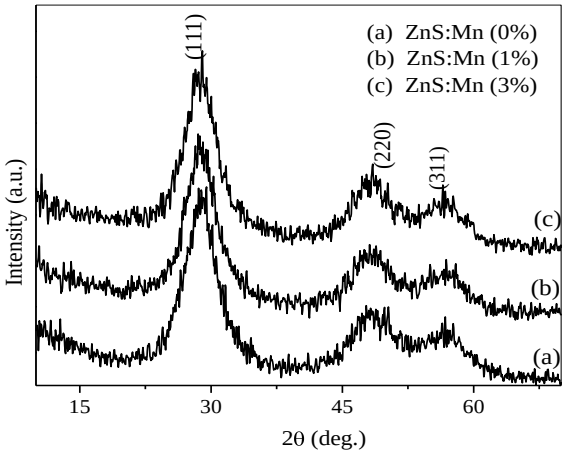

Fig. 1 *– XRD spectra of* $Zn_{1-x}Mn_xS$ *(*x = 0.00, 0.01 *and* 0.03*) nanoparticles*

Table 1 *– Parameters calculated from XRD data*

Samples	Lattice constant (Å)
ZnS:Mn (0%)	5.372
ZnS:Mn (1%)	5.348
ZnS:Mn (3%)	5.331

3.2 UV-Vis absorption studies

The UV-Vis absorption spectra given in Fig. 2, shows UV absorption peak of about 342 nm without any visible absorption, which is slightly blue shifted from bulk (345 nm). To get precise measure of absorption edge, first derivative of absorption spectra is taken and the point of inflection is considered as the absorption edge.

With increase of Mn concentration, slight shift in bandgap towards higher energy is observed as shown in Table 2. From the bandgap, the size of the nanoparticle was calculated by using Brus formula (Eqn. 1) which is valid only for the case of nanomaterials having bandgap blue shifted from bulk,

$$R^2 = \frac{2h^2 E_{gb}\pi^2}{(E^2_{gn} - E_{gb}{}^2)m^*} \qquad (1)$$

where R is the radius of nanoparticles, E_{gn} and E_{gb} are bandgap of nano and bulk system, respectively and m^* is the effective electron mass ($m^* = 0.34m_e$). The particle size was calculated as around ~ 24 nm for un-doped samples, which slightly decreased with increase of Mn doping concentration.

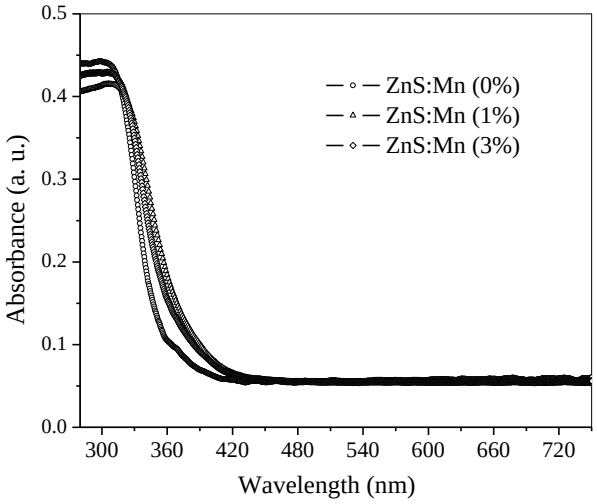

Fig. 2 *– UV-Vis absorption spectra of* $Zn_{1-x}Mn_xS$ *(*x = 0.00, 0.01 *and* 0.03*) nanoparticles*

Table 2 *– Bandgap calculated from UV- Vis absorption spectra*

Samples	Absorption edge (nm)	Bandgap (eV)
ZnS:Mn (0%)	342	3.63
ZnS:Mn (1%)	334	3.71
ZnS:Mn (3%)	332	3.73

3.3 Photoluminescence studies

Room temperature photoluminescence spectra of all the samples are given in Fig. 3 and shows emission peaks at 428 nm and 602 nm (since there is slight shift in UV absorption peak for doped samples from un-doped, all are excited at 340 nm). A schematic band diagram for Mn^{2+} doped ZnS nanomaterials are given in Fig. 4.

Blue emission observed at 428 nm are attributable to defect originated from sulfur vacancies (which is evident from EDS data), related to emission of ZnS host [14]. It is well-known that Mn^{2+} can substitute for Zn^{2+} ions in the ZnS crystal lattice because of their close ionic radii (0.80 and 0.83 Å for Mn^{2+} and Zn^{2+}, respectively).

So the orange emission (602 nm) observed in different Mn doped samples is the characteristics of Mn^{2+} and it is mainly due to its $^4T_1$-$^6A_1$ transition, compared to bulk ZnS:Mn (585 nm) [3]. Similarly, Goudarzi et al. [15] observed the characteristic emission of Mn^{2+} ions in ZnS crystals approximately at 590 nm (yellowish-orange) for the excitation of 320 nm. This results clearly suggest that emission at 602 nm (2.06 eV) arises from Mn^{2+} being incorporated from ZnS nanocrystals not from MnS, since the absence of secondary phase are already confirmed from XRD (It is important to note that the Mn^{2+} ions in MnS nanocrystals have two emission peaks at 1.66 and 1.80 eV). But noticeably, with the increase of Mn^{2+} concentration the intensity of the orange (Mn^{2+}) emission significantly increases while its

peak position does not shift, which is similar to the result of Peng et al. [7], but the intensity from the host lattice (blue) emission shows a slow increase. When Mn is doped, it may introduce inside of ZnS nanocrystals or to be added to the outside. Mn^{2+} incorporated into ZnS lattice leads to orange emission. ZnS with surface bound Mn^{2+} yields UV emission. Here, no UV emission was observed, so Mn^{2+} incorporated into ZnS only.

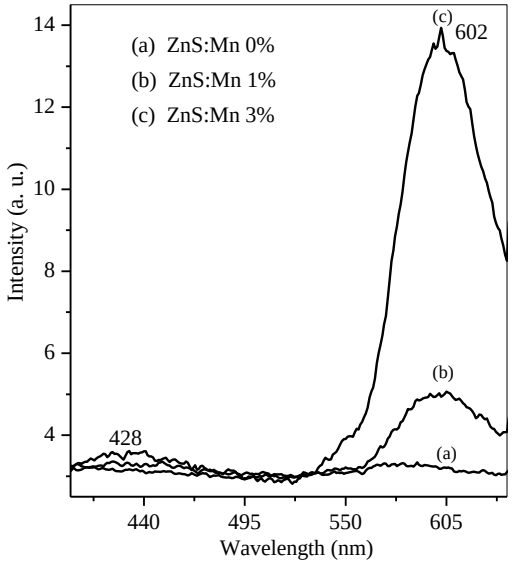

Fig. 3 *– Photoluminescence spectra of* $Zn_{1-x}Mn_xS$ *(*$x = 0.00$, 0.01 *and* 0.03*) nanoparticles*

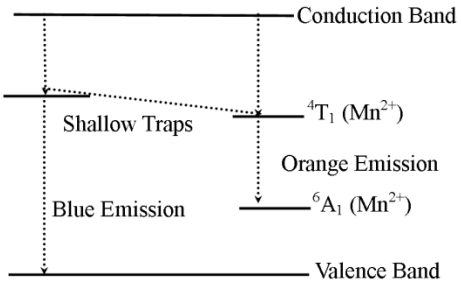

Fig. 4 *– A schematic band diagram for* Mn^{2+} *doped* ZnS *nanomaterials*

3.4 FTIR studies

FTIR spectra of undoped and Mn doped ZnS nanoparticles shows transmission band at 665 and 1113 cm^{-1} are assigned to the stretching vibrations of Zn-OH bond. In turn, the bonds at ~ 3388&1623, 1335, 920, and 620 cm^{-1} can be assigned to the stretching vibrations of O-H, C-H, CH_2, and C-S stretching vibration, respectively.

3.5 Compositional analysis

EDS spectra of undoped sample shows the presence of Zn and S elements alone in the sample and the doped samples includes Mn along with it, which confirms the absence of any other impurities. The atomic percentage of Zn and S elements in undoped ZnS sample differs from actual stoichiometric atomic percentage of Zn and S of 50% each, which shows sulfur vacancies in the synthesized sample (Table: 1). Likewise all the doped samples show sulfur deficiency. Even though, we intended to add 1 and 3at. % of Mn into ZnS, only 0.22 and 0.66 at. % of Mn were entered into the system and the remaining was washed away during the synthesis.

Table 3 *– Elemental composition of* $Zn_{1-x}Mn_xS$ *(*x = 0.00, 0.01 *and* 0.03*) nanoparticles from EDS*

Samples	Elements (at. %)		
	Zn	S	Mn
ZnS:Mn (0%)	63.83	36.17	-
ZnS:Mn (1%)	65.28	34.47	0.25
ZnS:Mn (3%)	67.73	31.62	0.66

3.6 Magnetic properties

Since it is confirmed that undoped and Mn doped ZnS nanoparticles were synthesized without any other external impurities, the magnetic properties of all the samples are now investigated by using vibrating sample magnetometer (VSM) at room temperature. The magnetization properties of ZnS nanoparticles with different Mn^{2+} concentrations in Fig. 5 show the antiferromagnetic with diamagnetic behavior for all the samples at room temperature. The coercivity values were increased upto 1 at% of Mn and decreases for 3 at.% and retentivity values were vice-versa, which were tabulated in Table 4. Similarly, Rashad et al. [16] recently observed the same behavior for Mn dopant above 30 % in ZnS system and this is mainly due to coupled antiferromagnetic interaction between Mn ions.

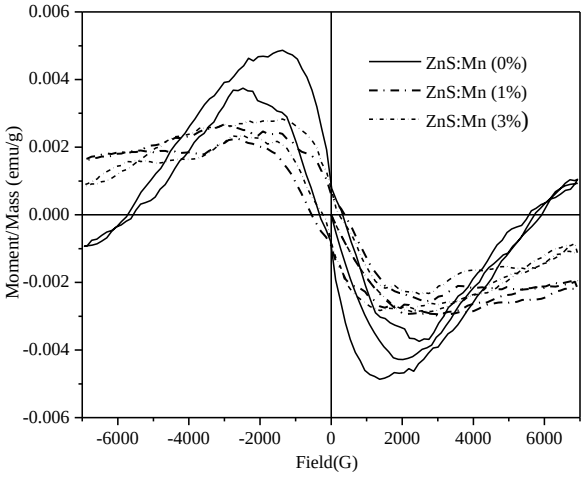

Fig. 5 *– VSM spectra of* $Zn_{1-x}Mn_xS$ *(*x = 0.00, 0.01 *and* 0.03*) nanoparticles*

Table 4 – *Magnetic parameters calculated from VSM spectra*

Samples	Coercivity (G)	Retentivity (emu/g)
ZnS:Mn (0%)	332.29	0.0092
ZnS:Mn (1%)	552.02	0.0062
ZnS:Mn (3%)	218.95	0.0078

4. CONCLUSION

ZnS nanoparticles doped with various Mn^{2+} concentration were synthesized through the co-precipitation method with the average size of around 2 nm, independent of Mn^{2+} doping. The XRD result reveals that the samples possess the cubic zinc blende structure of ZnS, without any manganese impurity. UV-Vis absorption peak shows blue shift from bulk with slight shift in bandgap due to Mn doping. Room temperature PL spectra exhibits two emission peaks, both of which can be attributed to ZnS host and Mn^{2+} ions respectively. The compositional analysis shows presence of Zn, S, and Mn in the corresponding system and absence of any other impurities. The magnetic measurements show that all the samples exhibit antiferromagnetic with diamagnetic behavior at room temperature.

The authors thank Madurai Kamaraj University for the award of University Stipendiary Research Fellowship (USRF), UGC-DRS and UPE for the financial support.

REFERENCES

1. S. Yanagida, H. Kawakami, Y. Midori, H. Kizumoto, C.J. Pac, Y. Wada, *Bull. Chem. Soc. Jpn*. **68**, 1811 (1995).
2. Y. Wada, H. Yin, T. Kitamura, S. Yanagida, *Chem. Commun*. **24**, 2683 (1998).
3. R.N. Bhargava, D. Gallagher, X. Hong, A. Nurmikko, *Phys. Rev. Lett*. **72**, 416 (1994).
4. I.I. Yu, M. Senna, *Appl. Phys. Lett*. **66**, 424 (1995).
5. T. Lgarashi, T. Lsabe, M. Senna, *Phys. Rev. B* **56**, 6444 (1997).
6. M. Konishi, T. Isobe, M. Senna, *J. Lumin*. **93**, 1 (2001).
7. W.Q. Peng, S.C. Qu, G.W. Cong, X.Q. Zhang, Z.G. Wang, *J. Crys. Grow*. **282**, 179 (2005).
8. Z.H. Wang, D.Y. Geng, D. Li, Z.D. Zhang, *J. Mater. Res*. **22**, 2376 (2007).
9. H. Heidrich, *phys. stat. sol. a* **67**, 163 (1981).
10. N. Tsujii, H. Kitazawa, G. Kido, *J. Appl. Phys*. **93**, 6957 (2003).
11. H.J. Yuan, X.Q. Yan, Z. X. Zhang, D.F. Liu, Z. P. Zhou, L. Cao, J.X. Wang, Y. Gao, L. Song, L. F. Liu, X.W. Zhao, X.Y. Dou, W. Y. Zhou, S.S. Xie, *J. Cryst. Growth* **271**, 403 (2004).
12. P.V.B. Lakshmi, K. Sakthiraj, K. Ramachandran, *Cryst. Res. Technol*. **44**, 153 (2008).
13. S.D. Han, K.C. Singh, H.S. Lee, T.Y. Cho, J.P. Hulme, C.H. Han, I.S. Chun, J. Gwak, *Mater. Chem. Phys*. **112**, 1083 (2008).
14. W.G. Becker, A.J. Bard, *J. Phys. Chem*. **87**, 4888 (1983).
15. A. Goudarzi, G.M. Aval, S.S. Park, M.C. Choi, R. Sahraei, M.H. Ullah, A. Avane, C.S. Ha, *Chem. Mater*. **21**, 2375 (2009).
16. M.M. Rashad, D.A. Rayan, K.E. Barawy, *J. Phys.: Conf. Series* **200**, 072077 (2010).